A fixed-lag Kalman smoother to filter power line interference in electrocardiogram recordings

A Fixed-Lag Kalman Smoother to Filter Power Line Interference in Electrocardiogram Recordings

G. J. J. Warmerdam*, R. Vullings, L. Schmitt, J. O. E. H. Van Laar, and J. W. M. Bergmans

***Abstract*—Objective: Filtering power line interference (PLI) from electrocardiogram (ECG) recordings can lead to significant distortions of the ECG and mask clinically relevant features in ECG waveform morphology. The objective of this study is to filter PLI from ECG recordings with minimal distortion of the ECG waveform. *Methods*: In this paper, we propose a fixed-lag Kalman smoother with adaptive noise estimation. The performance of this Kalman smoother in filtering PLI is compared to that of a fixed-bandwidth notch filter and several adaptive PLI filters that have been proposed in the literature. To evaluate the performance, we corrupted clean neonatal ECG recordings with various simulated PLI. Furthermore, examples are shown of filtering real PLI from an adult and a fetal ECG recording. *Results*: The fixed-lag Kalman smoother outperforms other PLI filters in terms of step response settling time (improvements that range from 0.1 to 1 s) and signal-to-noise ratio (improvements that range from 17 to 23 dB). Our fixed-lag Kalman smoother can be used for semi real-time applications with a limited delay of 0.4 s. *Conclusion and Significance*: The fixed-lag Kalman smoother presented in this study outperforms other methods for filtering PLI and leads to minimal distortion of the ECG waveform.**

***Index Terms*—Electrocardiography, Kalman filter (KF), Kalman smoother (KS), power line interference (PLI).**

I. Introduction

POWER line interference (PLI) is often a source of interference for biomedical signals such as electrocardiogram (ECG) recordings. Electric fields surrounding the power lines are picked up by the patient, the electric wires, and by the electrocardiograph itself. Differences in skin-electrode impedance of electrodes can lead to voltage differences measured at the electrodes which are then amplified at the output. Using a proper recording setup (e.g., cable shielding or amplifiers with a high common-mode rejection) can reduce PLI, but this is often insufficient to fully suppress PLI. Especially with developments in sensor technology in the direction of less obtrusive sensors such as textile electrodes and capacitive electrodes [1], PLI can even exceed the ECG in amplitude. Despite that filtering PLI is a fairly mature domain [2]–[10], filtering PLI from ECG recordings remains a challenging task because the frequency content of the ECG (in particular, the frequency content of the QRS complex) overlaps with the frequency of the PLI.

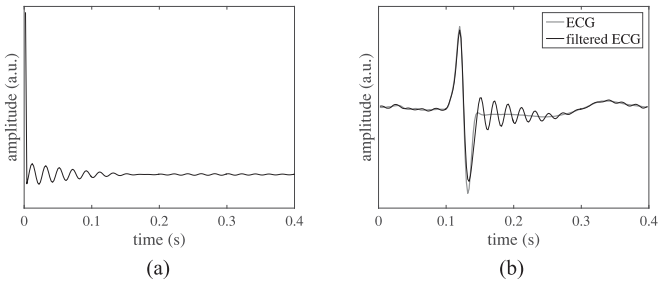

Fig. 1. Effect of fixed-bandwidth notch filter. (a) Impulse response of a second order IIR notch filter. (b) Clean neonatal ECG signal before and after notch filtering.

The classical approach for removing PLI is to use a fixed notch filter (e.g., an infinite impulse response (IIR) filter [11]), with unit gain at all frequencies except the PLI frequency. Typically, the impulse response of a notch filter shows some ringing [3], as presented in Fig. 1(a). In case of a steep QRS complex, this ringing effect is also observed after filtering an ECG signal with the fixed notch filter. In particular for neonatal and fetal ECG, ringing can lead to significant disturbance of the ECG, as shown in Fig. 1(b). The shorter duration of the QRS complex (typically 50 ms for neonates and 40 ms for fetuses) compared to the duration of the adult QRS complex (typically 80 ms) [12], leads to more overlap of the frequency content of the QRS complex with the frequency of the PLI. Note that since ringing is a response of the notch filter to a QRS complex, using a notch filter will always cause ringing, even in case there is little to no PLI in the recording.

As an alternative to notch filters with fixed parameters, several adaptive filters have been proposed in the literature [4]–[10]. Least-mean-square (LMS) adaptive algorithms were used in [4]–[8]. The first adaptive filters that were developed had the practical limitation that they required an externally recorded reference signal [4]–[6]. In contrast, an algorithm that

Manuscript received September 21, 2016; revised November 3, 2016; accepted November 4, 2016. Date of publication November 8, 2016; date of current version July 15, 2017. This work was supported by the IMPULS perinatology program. *Asterisk indicates corresponding author.*

*G. J. J. Warmerdam is with the Faculty of Electrical Engineering, Eindhoven University of Technology, Eindhoven 5612 AZ, The Netherlands (e-mail: g.j.j.warmerdam@tue.nl).

R. Vullings and J. W. M. Bergmans are with the Faculty of Electrical Engineering, Eindhoven University of Technology.

L. Schmitt is with the Philips Research.

J. O. E. H. Van Laar is with the Máxima Medical Center.

Digital Object Identifier 10.1109/TBME.2016.2626519

required no additional reference signal was suggested by Ziarani *et al.* [7]. In [8], Martens *et al.* made improvements to the algorithm of Ziarani, resulting in a more stable filter. More recently, some researchers have used a Kalman filter (KF) [9] and extended KF [10] for PLI tracking and cancellation. Unlike LMS algorithms that use a fixed learning rate, KFs have the advantage that the learning rate of the filter is adapted to the signal-to-noise ratio (SNR).

Although most of these studies also consider the possibility of frequency deviations of the PLI, frequency deviations are only of the order $\pm$ 0.01 Hz in most developed countries according to the power system quality standards [13]. In contrast to the relatively stable frequency, the amplitude and phase of the PLI can significantly change, e.g., due to different patient positioning or impedance changes. A linear KF was suggested by Sameni that combined variations in both amplitude and phase into the estimation of a single parameter [9]. This method has the advantage that it does not require *a priori* knowledge of the PLI amplitude and phase dynamics.

One of the main problems with adaptive filtering of PLI from ECG recordings is the interference of the QRS complex with the parameter estimation [6], [8]. While fast adaptation of model parameters is preferred in order to track changes in the PLI, using high learning rates will also allow model parameters to adapt to the QRS complex, hence leading to distortion of the ECG waveform. To prevent model parameters from adapting to the QRS complex, several studies have suggested to reduce the learning rate during a QRS complex or even set the learning rate to zero, either based on R-peak locations [6] or based on some general properties of the QRS complex [8]. Reducing the learning rate during a QRS complex has shown promising results. Unfortunately, in case of a time-varying PLI, this approach leads to an error in the estimation of the PLI after a QRS complex.

In this study, we suggest to use a Kalman smoother (KS) to improve estimation of the PLI. A smoother consists of a combination of two filters: one filter operates on past observations (called a forward filter), while the other filter operates on future observations (called a backward filter) [14]. Ideally, the forward and backward parameter estimation have uncorrelated errors and the combination of the two improves the parameter estimation [14], [15]. Besides the advantage of improving the parameter estimation, a KS also reduces the error made by the interference of QRS complexes with the parameter estimation. Because smoothing requires future information, a delay is generated in the estimation of the PLI. However, for most real-time applications, a small delay is acceptable. We, therefore, propose a fixed-lag KS that estimates the PLI for some fixed time lag [16].

The rest of this paper is organized as follows; in Sections II-A and II-B, the linear KF and extension to a fixed-lag KS are discussed. Noise estimation that accounts for the interference of the ECG with the parameter estimation of the PLI is discussed in Sections II-C and II-D. Then, Section III discusses the data acquisition and simulation of the PLI that is used to validate the developed method. For validation, we used neonatal ECG recordings, but the developed algorithm can equally be applied to adult and fetal ECG recordings, as is shown by two examples. Finally, our work is compared to several other algorithms proposed in the literature, and results and discussion are presented in Sections IV and V.

II. Methods

A. Linear Kalman Filter

Implementation of the linear KF is based on the work presented by Sameni [9]. This section summarizes the main concepts of the KF.

The PLI is modeled as a periodic signal with frequency (f_0), amplitude (B), and phase (ϕ)

$$x_n = B\cos(\omega_0 n + \phi) \tag{1}$$

where $\omega_0 = 2\pi f_0/f_s$ is the angular frequency, n the time index, and f_s the sampling frequency. Using basic trigonometry, the aforementioned equation can be rewritten into a recursive equation as follows:

$$x_{n+1} + x_{n-1} = 2\cos(\omega_0)x_n\,. \tag{2}$$

To approximate variations in amplitude, phase, or frequency between x_{n+1} and x_n an additive random term w_n is used, which will be referred to as process noise. Although variations in phase and frequency are not additive, this approximation works well in practice since variations in phase and frequency are relatively small for PLI [13]. To obtain an analytically tractable solution for the parameter estimation, w_n is assumed to be a zero-mean Gaussian distribution with variance q_n. The PLI model can hence be expressed as

$$x_{n+1} + x_{n-1} = 2\cos(\omega_0)x_n + w_n\,. \tag{3}$$

The recorded signal (y_n) does not only consists of PLI, but contains a superposition of several other signals such as the ECG, the electromyogram, and noise. All non-PLI signals are represented by a random noise term v_n, which will be referred to as observation noise. The signal recorded at the electrodes is thus modeled as

$$y_n = x_n + v_n\,. \tag{4}$$

Because v_n is considered a combination of several signals, including measurement noise, we assumed v_n to have a zero-mean Gaussian distribution with variance r_n. Note that since v_n also models the ECG, this assumption is only approximately true. However, in [16], it is shown that even in case of non-Gaussian noise, a KF is the optimal linear estimator in the sense that it minimizes the mean square error.

Based on (3) and (4), we can define a state-space model that describes the PLI as follows:

$$\begin{aligned} \vec{x}_{n+1} &= \mathbf{A}\vec{x}_n + \vec{b}w_n \\ y_{n+1} &= \vec{h}^T\vec{x}_{n+1} + v_{n+1} \end{aligned} \tag{5}$$

where

$$\vec{x}_n = \begin{bmatrix} x_n \\ x_{n-1} \end{bmatrix}, \mathbf{A} = \begin{bmatrix} 2\cos(\omega_0) & -1 \\ 1 & 0 \end{bmatrix}, \vec{b} = \begin{bmatrix} 1 \\ 0 \end{bmatrix}, \text{ and } \vec{h} = \begin{bmatrix} 1 \\ 0 \end{bmatrix}.$$

Given observations y_{n+1}, our aim is to estimate the parameter $\vec{x}_{n+1}$. The first element of the estimate of $\vec{x}_{n+1}$ is then our estimation of the PLI at time $n+1$. Due to the uncertainties in the state-space model described by (5), a probabilistic approach can be used to solve the PLI estimation problem. In this case, we are interested in $\vec{x}_{n+1}$ that maximizes the *posterior* probability density function $p(\vec{x}_{n+1}|y_{n+1}, I)$, with $I = \{\mathbf{A}, \vec{b}, \vec{h}, q_n, r_n\}$.

According to Bayes' rule, we can describe the PLI parameter estimation problem as

$$p(\vec{x}_{n+1}|y_{n+1}, I) = \frac{p(y_{n+1}|\vec{x}_{n+1}, I)p(\vec{x}_{n+1}|y_n, I)}{p(y_{n+1}|y_n, I)}. \quad (6)$$

Due to the assumption of Gaussian process and measurement noise, the posterior is a Gaussian distribution and it is fully described by its mean $\hat{\vec{x}}_{n+1|n+1}$ and its associated covariance $\mathbf{P}_{n+1|n+1}$. The notation $\hat{\vec{x}}_{n+1|n+1}$ represents the estimation of $\vec{x}$ at time $n+1$, given observations $Y = \{y_1, y_2, ..., y_{n+1}\}$.

Using a similar derivation as described in [17], the maximum *a posteriori* (MAP) estimate of the PLI $\hat{\vec{x}}_{n+1|n+1}$ and its covariance $\mathbf{P}_{n+1|n+1}$ can sequentially be updated according to the KF equations, given by

$$\hat{\vec{x}}_{n+1|n+1} = \mathbf{A}\hat{\vec{x}}_{n|n} + \vec{K}_n(y_{n+1} - \vec{h}^T\mathbf{A}\hat{\vec{x}}_{n|n}) \quad (7)$$

$$\mathbf{P}_{n+1|n+1} = \mathbf{A}\mathbf{P}_{n|n}\mathbf{A}^T + q_n\vec{b}\vec{b}^T - \vec{K}_n\vec{h}^T(\mathbf{A}\mathbf{P}_{n|n}\mathbf{A}^T + q_n\vec{b}\vec{b}^T) \quad (8)$$

and $\vec{K}_n$ the Kalman gain [18]

$$\vec{K}_n = \frac{(\mathbf{A}\mathbf{P}_{n|n}\mathbf{A}^T + q_n\vec{b}\vec{b}^T)\vec{h}}{\vec{h}^T(\mathbf{A}\mathbf{P}_{n|n}\mathbf{A}^T + q_n\vec{b}\vec{b}^T)\vec{h} + r_{n+1}}. \quad (9)$$

After estimating the PLI, the ECG signal is obtained by the innovation signal of the KF as

$$\hat{v}_{n+1} = y_{n+1} - \hat{x}_{n+1|n+1} \quad (10)$$

where $\hat{x}_{n+1|n+1}$ is the first element of $\hat{\vec{x}}_{n+1|n+1}$.

B. Fixed-Lag Kalman Smoother

The KF update equations described by (7)–(9) provide causal estimations of the PLI, which means that at time $n+1$, they yield estimates given all past observations and the current observation (Y). While for real-time applications, causality is required, for most applications, a small delay of τ samples is often acceptable to improve the estimation accuracy. When appropriately designed, the combination of a causal filter and a backward filter that uses future information results in smaller estimation errors compared to the causal filter alone [14], [15].

Our goal is to estimate $\hat{\vec{x}}_{n-\tau|n+1}$ for some fixed time-lag τ. In other words, we want to estimate the state at time $n-\tau$, given past observations $\{y_1, ..., y_{n-\tau}\}$ and future observations $\{y_{n-\tau+1}, ..., y_{n+1}\}$. The key concept is to define an augmented state vector $\vec{X}^a \in \mathbb{R}^{2(\tau+1)}$ [16]

$$\vec{X}^a_{n+1} = \begin{bmatrix} \vec{x}^{(0)}_{n+1} \\ \vec{x}^{(1)}_{n+1} \\ \vdots \\ \vec{x}^{(\tau+1)}_{n+1} \end{bmatrix} = \begin{bmatrix} \mathbf{A} & 0 & \cdots & 0 \\ \mathbf{I}_2 & 0 & \cdots & 0 \\ 0 & \mathbf{I}_2 & \cdots & 0 \\ \vdots & \vdots & \cdots & \vdots \\ 0 & \cdots & \mathbf{I}_2 & 0 \end{bmatrix} \begin{bmatrix} \vec{x}^{(0)}_n \\ \vec{x}^{(1)}_n \\ \vdots \\ \vec{x}^{(\tau+1)}_n \end{bmatrix} + \begin{bmatrix} \vec{b} \\ 0 \\ \vdots \\ 0 \end{bmatrix} w_n \quad (11)$$

with $\mathbf{I}_2$ is the $[2 \times 2]$ identity matrix and element $\vec{x}^{(i)}_{n+1}$ is the ith time lag of $\vec{x}_{n+1}$.

From (11), we can see that, except for the first component, the components of the augmented vector $\vec{X}^a_{n+1}$ are sequentially delayed versions of the previous augmented vector $\vec{X}^a_n$. Moreover, if we initialize $\vec{x}^{(0)}_n$ as the state at time n of the original system described by (5), we observe that the first row of the augmented system describes the original system, while the remaining rows give successive time delays. The last component of the estimate $\hat{\vec{X}}^a_{n+1|n+1}$ is $\hat{\vec{x}}_{n-\tau|n+1}$, which is the estimate we are looking for.

Based on the augmented state vector, we can obtain an augmented state-space model as

$$\begin{aligned} \vec{X}^a_{n+1} &= \mathbf{A}^a\vec{X}^a_n + \vec{B}^a w_n \\ y_{n+1} &= \vec{H}^{a^T}\vec{X}^a_{n+1} + v_{n+1} \end{aligned} \quad (12)$$

with model parameters defined as

$$\mathbf{A}^a = \begin{bmatrix} \mathbf{A} & 0 & \cdots & 0 \\ \mathbf{I}_2 & 0 & \cdots & 0 \\ 0 & \mathbf{I}_2 & \cdots & 0 \\ \vdots & \vdots & \cdots & \vdots \\ 0 & \cdots & \mathbf{I}_2 & 0 \end{bmatrix}, \vec{B}^a = \begin{bmatrix} \vec{b} \\ 0 \\ \vdots \\ 0 \end{bmatrix}, \text{ and } \vec{H}^a = \begin{bmatrix} \vec{h} \\ 0 \\ \vdots \\ 0 \end{bmatrix}.$$

Since the augmented state-space model in (12) again describes a linear dynamic system, we can use the same reasoning as used in Section II-A to obtain an MAP solution for the augmented system

$$\hat{\vec{X}}^a_{n+1|n+1} = \mathbf{A}^a\hat{\vec{X}}^a_{n|n} + \vec{K}^a_n(y_{n+1} - H^{a^T}\mathbf{A}^a\hat{\vec{X}}^a_{n|n}) \quad (13)$$

$$\mathbf{P}^a_{n+1|n+1} = \mathbf{A}^a\mathbf{P}^a_{n|n}\mathbf{A}^{a^T} + q_n\vec{B}^a\vec{B}^{a^T} - \vec{K}^a_n\vec{H}^{a^T}(\mathbf{A}^a\mathbf{P}^a_{n|n}\mathbf{A}^{a^T} + q_n\vec{B}^a\vec{B}^{a^T}) \quad (14)$$

and the augmented Kalman gain

$$\vec{K}^a_n = \frac{(\mathbf{A}^a\mathbf{P}^a_{n|n}\mathbf{A}^{a^T} + q_n\vec{B}^a\vec{B}^{a^T})\vec{H}^a}{\vec{H}^{a^T}(\mathbf{A}^a\mathbf{P}^a_{n|n}\mathbf{A}^{a^T} + q_n\vec{B}^a\vec{B}^{a^T})\vec{H}^a + r_{n+1}}. \quad (15)$$

A drawback of using update equations (13)–(15) is that it requires computation of a $[2(\tau+1) \times 2(\tau+1)]$ covariance

matrix $\mathbf{P}^a_{n|n}$ at each time instant n. This can become computationally expensive for increasing time delay or for high sampling rates. However, it is possible to show by expansion of the matrix products in (13)–(15) that only the first column of the covariance matrix is required to calculate the smoothed estimate $\hat{\vec{x}}_{n-\tau|n+1}$ and Kalman Gain $\vec{K}^a_n$, greatly decreasing computational complexity [16].

C. Preprocessing

For optimal performance of the KS, the observation noise should be white [16]. In our model, the observation noise represents all non-PLI signals, and thus, also contains correlated physiological noise, most importantly, the ECG. Ideally, a whitening filter should be implemented that ensures that the innovation signal is white. However, for ECG recordings, it is difficult to design such a whitening filter due to the nonstationary frequency content of the ECG (i.e., P-wave, QRS complex, and T-wave have different frequency contents).

Because the ECG has a low-frequency nature (in particular, the P- and T-wave), we used a high-pass filter that serves to crudely whiten the innovation signal [8]. To this end, observations y are first preprocessed with the high-pass filter to obtain $\tilde{y}$. Since the frequency content of the P- and T-wave is generally low compared to the PLI frequency [19], the high-pass filter can be designed to suppress the P- and T-wave, while leaving the PLI undisturbed. As a result, the new innovation signal of the KS $\hat{\tilde{v}}_{n+1} = \tilde{y}_{n+1} - \hat{x}_{n+1|n+1}$ no longer contains the P- and T-wave.

We used a linear phase finite impulse response (FIR) filter with 40 coefficients and a cutoff frequency of 30 Hz. The FIR filter has unit gain at the PLI frequency and a group delay of half of the length of the filter. To correct for the group delay, the first 20 samples of the PLI estimation are discarded.

D. Noise Estimation

Sameni showed that under assumption of stationary observation and process noise ($r_n = r$ and $q_n = q$), the KF described in Section II-A converges to a second-order notch filter [9]. When the amplitude or phase of the PLI varies, or in case of nonstationary observation noise, this assumption is incorrect and the KF performs suboptimally.

1) Observation Noise: In contrast to the frequency content of the P- and T-wave, the frequency content of the QRS complex overlaps with the PLI frequency. Therefore, a high-pass filter is not able to fully suppress the QRS complex with respect to the PLI and $\tilde{y}$ still contains remainders of the QRS complex. Due to the remainders of the QRS complex, the variance in the observation noise is time-varying and increases during a QRS complex. Moreover, remainders of the QRS complex also cause a temporal increase in the correlation of $\tilde{y}$. Hence, the innovation signal $\hat{\tilde{v}}$ will be less white during a QRS complex, reducing the performance of the parameter estimation by the KS.

From (9), we can see that an increase in r_{n+1} will lead to a decrease in $\vec{K}_n$. In turn, from (7), we can observe that for low

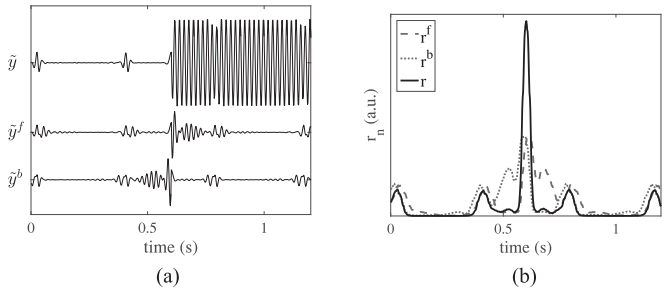

Fig. 2. Estimation of the observation noise r_n.

$\vec{K}_n$, a new estimation of the PLI ($\hat{\vec{x}}_{n+1|n+1}$) will mostly depend on the a priori estimate ($\mathbf{A}\hat{\vec{x}}_{n|n}$) and less on observation $\tilde{y}_{n+1}$. Therefore, to reduce the influence of the remainders of the QRS complex on the parameter estimation, it is important to include in our method a time-varying estimation of r_{n+1}.

Since r_{n+1} represents the variance of the signal without PLI, it can be estimated based on the signal that remains after passing $\tilde{y}$ through a forward coarse fixed-bandwidth notch filter ($\tilde{y}^f$). However, after a sudden change in PLI (e.g., a step increase in amplitude), $\tilde{y}^f$ will be contaminated by some remaining PLI due to the response time of the fixed-bandwidth notch filter, as shown in Fig. 2(a). As a consequence, if r_{n+1} is estimated based on $\tilde{y}^f$, the value of r_{n+1} will increase after a sudden change in PLI. In turn, the increase in r_{n+1} leads to a decrease in $\vec{K}_n$, while actually an increase in $\vec{K}_n$ is required for fast adaptation of the KS model parameters to the changes in PLI.

Instead of estimating r_{n+1} only based on $\tilde{y}^f$, we estimate r_{n+1} based on a combination of $\tilde{y}^f$ and a backward fixed-bandwidth notch filter (denoted as $\tilde{y}^b$). If a sudden change in PLI occurs at time t, $\tilde{y}^f$ has no remaining PLI before time t, while $\tilde{y}^b$ has no remaining PLI after time t, as shown in Fig. 2(a). Combining information from $\tilde{y}^f$ and $\tilde{y}^b$ leads to an accurate estimation of r_{n+1}, except at time t.

By taking the sum of absolute values for $\tilde{y}^f$ and $\tilde{y}^b$ over a time window M that corresponds to the length of a QRS complex, the amplitudes of the resulting signals are expected to be higher during a QRS complex with respect to other parts of the signals. We thus estimate the observation noise as

$$\hat{r}_n = \frac{1}{M}\sum_{j=n-M/2}^{n+M/2}\left|\tilde{y}^f_j\right| \cdot \frac{1}{M}\sum_{j=n-M/2}^{n+M/2}\left|\tilde{y}^b_j\right|. \qquad (16)$$

As fixed-bandwidth notch filter we use a second-order Butterworth notch filter, with cutoff frequencies of 45 and 55 Hz. Note that the approach described previously requires a delay τ^{fb} to compute $\tilde{y}^b$. Because $\hat{r}_{n+1}$ needs to be calculated in order to obtain the smoothed estimate of the PLI at time $n-\tau$, the delay τ^{fb} is in addition to the delay τ of the fixed-lag KS.

2) Process Noise: As noted by Sameni, the ratio between the observation and process noise ($\gamma_n = q_n/r_n$) is related to the quality factor (Q-factor) of the KF described in Section II-A [9]. Low γ_n is related to a high Q-factor and a narrow bandwidth

notch filter. High γ_n is related to a low Q-factor and a broad bandwidth notch filter.

Similar to [9], an average value $\bar{\gamma}$ is chosen and $\bar{\gamma}$ is then adjusted to variations in SNR. Variations around $\bar{\gamma}$ are based on the ratio between the variance of the innovation signal and the estimated variance of the innovation signal by the KS [9]. The value of γ_n is estimated as

$$\hat{\gamma}_n = \bar{\gamma} \cdot \frac{\hat{\tilde{v}}_n^2}{\vec{h}^T(\mathbf{A}\mathbf{P}_{n-1|n-1}\mathbf{A}^T + q_{n-1}\vec{b}\vec{b}^T)\vec{h} + \hat{r}_n}. \quad (17)$$

The process covariance q_n can then be estimated as the product of $\hat{\gamma}_n$ and $\hat{r}_n$. However, as discussed in Section II-D1, both $\hat{r}_n$ and $\hat{\tilde{v}}_n$ increase during a QRS complex, due to remainders of the QRS complex in $\tilde{y}$. This means that the process noise also increases during a QRS complex, leading to a faster adaptation of parameters. To prevent this unwanted effect, we used a moving average window with length L to calculate the process noise as

$$\hat{q}_n = \frac{1}{L}\sum_{j=n-L+1}^{n} \hat{r}_j \cdot \frac{1}{L}\sum_{j=n-L+1}^{n} \hat{\gamma}_j. \quad (18)$$

The value of L should be chosen longer than an interbeat interval so that $\hat{r}_n$ and $\hat{\gamma}_n$ are averaged over multiple heartbeats. Values of $\bar{\gamma}$ and L were empirically determined and set to $\bar{\gamma} = 1 \times 10^{-3}$ and $L = 1$ s.

E. Harmonics

The fixed-lag KS can easily be extended to also suppress the harmonics of the PLI. Since the harmonics are well separated in the frequency domain, it is possible to design a separate KS for each harmonic. Each KS will only affect its corresponding notch frequency and will not interfere with the estimation of a different harmonic.

F. Other Methods for PLI Suppression

For comparison, several other methods from the literature for removal of PLI have been implemented. We selected representative methods that use a different approach for suppression of the PLI. To this end, we implemented a fixed notch filter, an LMS based filter, and the KF described in Section II-A. These methods are only briefly discussed in this section. Settings for the algorithms were empirically determined and optimized for this study.

For the fixed notch filter, we used a second-order IIR Butterworth filter [11]. Fixed notch filters suppress a predetermined frequency range. For the selection of the cutoff values of the stopband, one should account for the distortion of the filter on the ECG and the ability of the filter to suppress a time-varying PLI. Selecting a narrow stop band generally causes less distortion of the ECG, however this leads to problems whenever the PLI is unstable. We used a stop band with cutoff values of $f_0 \pm 2$ Hz.

The performance of the fixed notch filter can be improved by filtering the signal in the backwards direction after filtering the signal in the forward direction. Since the fixed notch filter used in this paper is a linear time-invariant filter, any phase distortion of the ECG caused by the forward filter will be canceled out by the backward filtering [20]. Moreover, the amplitude response is squared, meaning that the attenuation in dB is doubled in the stop band. Although forward-backward filtering is generally used for offline applications, it is possible to implement it with some time delay for semi real-time applications. We set the delay similar to the delay τ^{fb} of the backward filter used to estimate r_n in Section II-D1.

Besides the fixed notch filter, we also implemented the LMS-based improved adaptive canceller (IAC), that was developed by Martens *et al.* [8]. The IAC algorithm is able to track amplitude, phase, and frequency changes of the PLI, with frequency deviations up to 4 Hz. Moreover, the method accounts for the interference of the QRS complex in the parameter estimation. Martens showed that performance of the IAC was superior to other adaptive algorithms for PLI suppression and this algorithm is thus used to represent adaptive filters. In the study of Martens, separate learning rates were derived for the amplitude (K_a), phase (K_ϕ), and frequency (K_ω) of the PLI. We used similar values for K_ϕ and K_ω as suggested in this paper. However, we noticed that K_a was too low and often parameter estimation of the PLI did not converge. Therefore, the value of K_a was empirically determined and increased from 8 s^{-1} to 100 s^{-1}.

Finally, we also compared our results to the results of the linear KF that was developed by Sameni [9]. Since this algorithm is described in Section II-A, we do not further discuss it here. In contrast to the KS, the KF suggested in [9] does not use a time-varying estimation of the observation noise to account for the ECG. Instead, the observation noise is estimated as the variance of the signal that remains after filtering y with a fixed-bandwidth notch filter. We used the same settings for the KF as for the fixed-lag KS ($\bar{\gamma} = 1e^{-3}$ and $L = 1$ s).

III. Data Acquisition

A. Simulated PLI

To validate our method, a dataset of ten neonatal ECG recordings was used. Signals were acquired at the Máxima Medical Center (Veldhoven, The Netherlands) and were recorded with a sample rate of 500 Hz. From each recording, a segment of one minute was selected. Because the signals were recorded with adhesive electrodes in a controlled environment, we were able to select segments with clean neonatal ECG that did not show any PLI.

The clean ECGs were then corrupted by simulated PLI. Depending on the country, f_0 can be either 50 or 60 Hz. We used 50 Hz for the simulations since this is used in European countries, but methods work similarly for 60 Hz. Algorithms were evaluated for several conditions of PLI: a PLI with a step increase and decrease in amplitude, a constant PLI, and a PLI with sinusoidal modulated amplitude at a frequency of 0.2 Hz to represent respiratory coupled changes.

In order to simulate similar SNR conditions of the clean ECG signals (s_n) with respect to the PLI (x_n) for all recordings, we normalized the ECG signals to unit power. The amplitude of the

PLI was then determined based on the SNR as

$$S_{\text{in}} = 10\log_{10}\left(\frac{P_s}{P_x}\right) \tag{19}$$

where P_s is the power of the ECG signal and P_x is the power of the PLI. PLI was simulated for different S_{in}, ranging from -20 to 20 dB. A step increase in PLI amplitude was simulated by decreasing the SNR from ∞ (PLI amplitude of 0 V) to S_{in}. A step decrease in PLI amplitude was simulated by increasing the SNR from S_{in} to ∞ (PLI amplitude of 0 V). Similarly, PLI with sinusoidal amplitude was simulated by modulating the SNR from ∞ (PLI amplitude of 0 V) to S_{in}.

Besides varying S_{in}, we also considered the influence of frequency deviations from the theoretical PLI frequency. For this purpose, we simulated PLI with frequency deviations up to $\Delta f = \pm 0.1$ Hz, at a S_{in} of -20 dB. We did not separately simulate a phase shift in the PLI, since simulating a frequency deviation from the PLI frequency is equivalent to a phase shift that increases linearly over time by $\Delta f \cdot n$.

B. Real PLI

Besides simulated PLI, we evaluated the performance of our method for recordings that are contaminated by real PLI. To show that the developed method is not limited to neonatal ECG applications, we used an adult and a fetal ECG recording as examples. Both recordings were obtained from abdominal ECG recordings, acquired at the Máxima Medical Center (Veldhoven, The Netherlands). For the fetal ECG, the abdominal signal was first preprocessed to suppress the maternal ECG using a dynamic template subtraction method [21].

C. Evaluation Criteria

To evaluate the performance of the algorithms, several evaluation criteria were used.

1) Settling Time: To quantify the step response of the algorithms, we used the settling time [22]. The settling time is defined as the time required for the error of the estimation of the PLI to settle within 5% of the step increase or decrease in amplitude. The first of 100 samples for which the error was under 5% for the full 100 samples was selected as the settling time.

For causal filters such as IAC and KF, once parameter estimation has converged before the step increase or decrease, only an error is seen in the parameter estimation after the step. In contrast, the KS and the forward-backward filtering of IIR will also show an error before the step increase or decrease. Therefore, we used the sum of the settling time before and after the step as the total settling time.

2) Output SNR: To evaluate the performance of the algorithms for ECGs that were corrupted with constant PLI and PLI with sinusoidal amplitude modulation, we used the SNR at the output of the filters. Similar to the definition of S_{in}, the SNR at the output was defined as

$$S_{\text{out}} = 10\log_{10}\left(\frac{P_s}{P_z}\right) \tag{20}$$

with $z = x - \hat{x}$, which represents the remaining PLI. To calculate P_z, the first and final second of z were excluded. Otherwise, results might be influenced by initialization effects that are unrelated to the type of simulated PLI (i.e., constant amplitude or PLI with sinusoidal amplitude modulation).

3) Computational Complexity: To measure the computational complexity, we used the number of multiplications per sample (MPS) after the initialization phase of the algorithms. Because for most digital signal processors (DSPs) the complexity of additions and subtractions is negligible compared to multiplications, additions and subtractions were not considered.

IV. Results

The fixed-lag KS and the methods described in Section II-F were implemented in MATLAB. The time delays of the KS and forward-backward IIR were determined empirically and both were set to 0.2 s (100 samples). The total delay of the KS, therefore, is $\tau^{\text{fb}} + \tau = 0.4$ s. The computational complexity of the KS depends on its time delays. Based on our implementation of the KS, we empirically determined that the computational complexity is equal to $10 + 10\tau^{\text{fb}} + 16\tau$, which is in the order of 10^3 MPS.

Fig. 3 shows examples of the output of the PLI filters for a neonatal ECG recording that is corrupted by simulated PLI with a step increase and decrease in amplitude, a constant PLI, and a PLI with sinusoidal amplitude modulation. In each example, PLI was simulated at $S_{\text{in}} = -20$ dB and $\Delta f = 0$ Hz. Fig. 4 shows examples of the output of the PLI filters for an adult and a fetal ECG recording that are corrupted by real PLI.

Table I shows the average settling time for a step increase and decrease in PLI amplitude. Tables II–IV show the average performance for different segments of the ECG (P-wave, QRS complex, and T-wave) under different PLI conditions. We defined the QRS complex as a segment of size M surrounding the R-peak (i.e., 80 ms for adult and 40 ms for fetal ECG [12]). The P-wave was defined as the segment before the start of the QRS complex and the T-wave as the segment after the end of the QRS complex. Table II shows average S_{out} if there is no PLI, Table III for PLI with constant amplitude, and Table IV for PLI with sinusoidal amplitude modulation. All values are expressed as mean $\pm$ standard deviation.

The effect of varying S_{in} on the S_{out} is shown in Fig. 5 and the effect of varying the frequency deviation from the theoretical PLI frequency is shown in Fig. 6.

V. Discussion

Filtering PLI from ECG recordings can lead to significant distortions of the ECG waveform. Traditional fixed-bandwidth notch filters distort the ECG by ringing due to the overlap of the frequency content of the QRS complex with the PLI frequency. As an alternative to suppress PLI, adaptive filtering techniques can be used. However, the ECG often interferes with the parameter estimation of the adaptive filters, also leading to distortion of the ECG waveform. In this study, the problem of interference of the ECG with parameter estimation was solved by implementation of a fixed-lag KS in combination with an adaptive noise

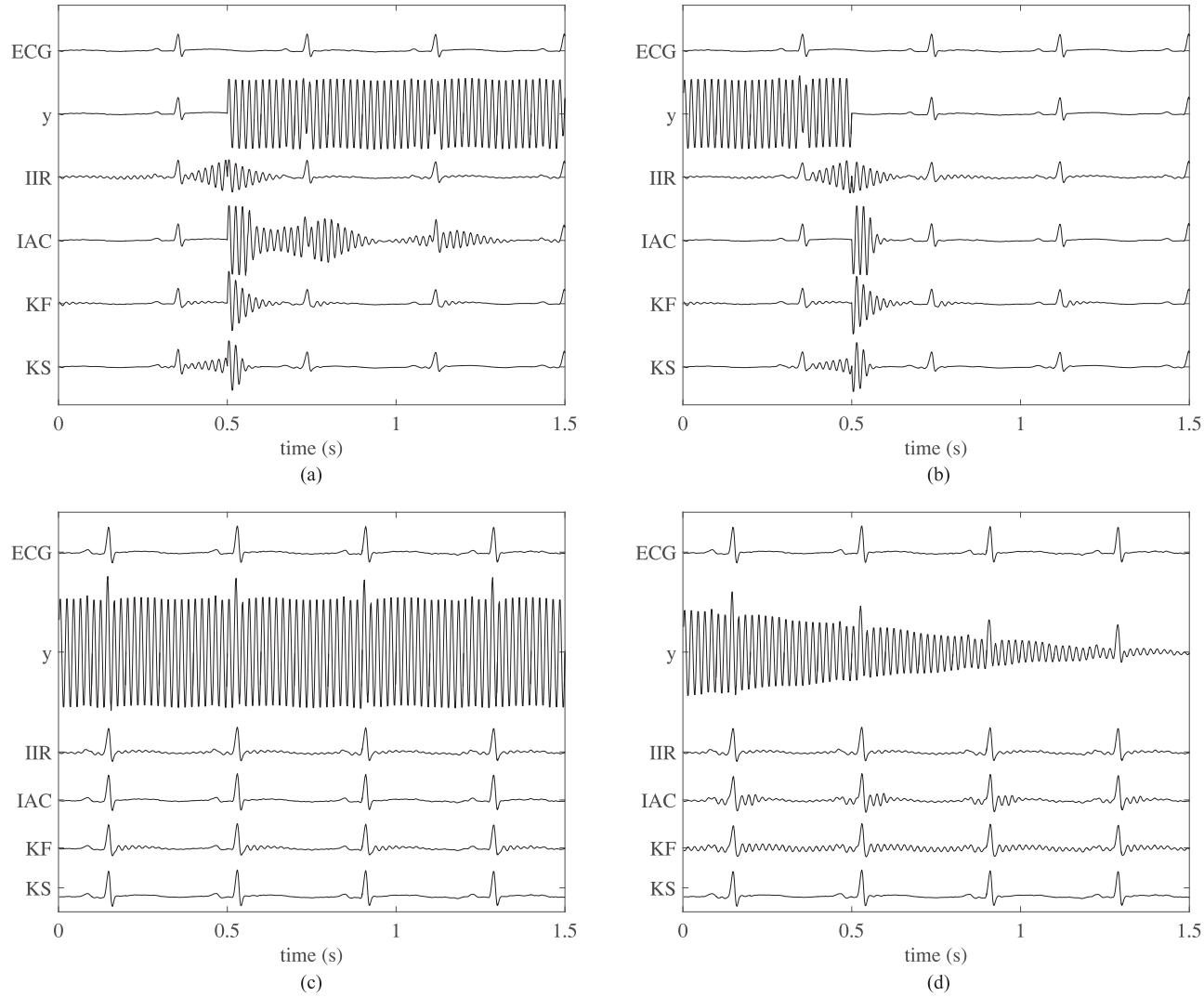

Fig. 3. Examples for a neonatal ECG recording corrupted with simulated PLI. The following signals are depicted: ECG is the original recording, *y* is the recording corrupted by simulated PLI, and IIR to the KS are the results of the filters. (a) Step increase. (b) Step decrease. (c) Constant amplitude. (d) Sinusoidal amplitude.

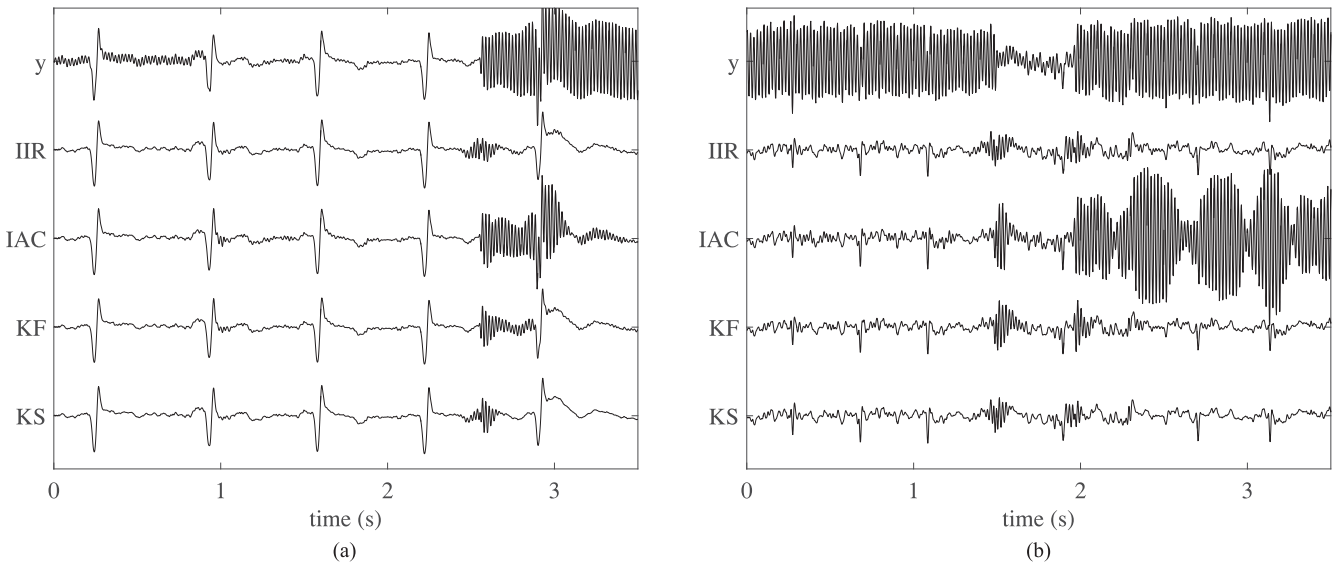

Fig. 4. Examples for an adult and a fetal ECG recording with real PLI. (a) Adult ECG (with $M = 80$ ms). (b) Fetal ECG (with $M = 40$ ms).

TABLE I
SETTLING TIME FOR A STEP INCREASE AND DECREASE IN PLI AMPLITUDE ($S_{\text{in}} = -20$ dB AND $\Delta f = 0$ Hz)

Algorithm	Amplitude Increase (s)	Amplitude Decrease (s)
IIR	0.26 ± 0.01	0.27 ± 0.06
IAC	1.15 ± 0.23	$\mathbf{0.14 \pm 0.06}$
KF	0.22 ± 0.10	0.22 ± 0.10
KS	$\mathbf{0.16 \pm 0.07}$	$\mathbf{0.14 \pm 0.03}$

TABLE II
S_{out} IN ABSENCE OF PLI ($S_{\text{in}} = \infty$)

Algorithm	Overall	P-Wave	QRS Complex	T-wave
IIR	20 ± 3	20 ± 3	16 ± 4	21 ± 4
IAC	$\mathbf{38 \pm 5}$	$\mathbf{40 \pm 6}$	$\mathbf{42 \pm 6}$	$\mathbf{40 \pm 5}$
KF	17 ± 3	35 ± 4	11 ± 3	18 ± 4
KS	37 ± 5	36 ± 4	36 ± 5	39 ± 5

TABLE III
S_{out} FOR CONSTANT PLI AMPLITUDE ($S_{\text{in}} = -20$ dB AND $\Delta f = 0$ Hz)

Algorithm	Overall	P-wave	QRS Complex	T-wave
IIR	20 ± 3	20 ± 3	16 ± 4	21 ± 4
IAC	34 ± 4	$\mathbf{36 \pm 5}$	35 ± 5	36 ± 4
KF	17 ± 3	35 ± 4	11 ± 3	18 ± 4
KS	$\mathbf{37 \pm 5}$	$\mathbf{36 \pm 4}$	$\mathbf{36 \pm 5}$	$\mathbf{41 \pm 6}$

TABLE IV
S_{out} FOR SINUSOIDAL PLI AMPLITUDE ($S_{\text{in}} = -20$ dB AND $\Delta f = 0$ Hz)

Algorithm	Overall	P-Wave	QRS Complex	T-Wave
IIR	20 ± 3	20 ± 3	16 ± 4	21 ± 4
IAC	7 ± 2	15 ± 1	7 ± 1	10 ± 1
KF	9 ± 1	12 ± 0	7 ± 1	11 ± 1
KS	$\mathbf{30 \pm 2}$	$\mathbf{32 \pm 3}$	$\mathbf{26 \pm 2}$	$\mathbf{35 \pm 4}$

estimation. The examples in Figs. 3 and 4 show that the proposed method can be used for filtering PLI from adult, neonatal, and fetal ECG recordings.

A. Step Response

We quantified the step response of the filters based on the settling time. From the examples in Fig. 3(a) and 3(b), it can be observed that the output of the forward-backward IIR filter and KS are also affected by the step increase and decrease in the period before the step occurs.

Overall, the KS has the shortest settling time for both a step increase and decrease in PLI amplitude (0.16 and 0.14 s, respectively), as shown in Table I. Although the settling time of the IAC was similar for a step decrease (0.14 s), the settling time for a step increase was much longer (1.15 s). Slower convergence of the IAC for a step increase was also observed by Martens [8]. This is partially due to the fact that the IAC requires separate estimation of the amplitude and phase of the PLI. Since both are unknown before the step increase, a longer period is required for the filter to converge. The KF and KS do not have this problem, because amplitude and phase variations are combined into a single parameter.

Although KS uses a fixed-bandwidth notch filter to estimate observation noise r_n, the settling time of the KS is shorter than the settling time of IIR (0.27 and 0.29 s for step increase and decrease, respectively). From Fig. 3(a) and 3(b), it can be seen that a fixed-bandwidth notch filter performs suboptimal during a step in PLI amplitude, which would in turn result in a poor estimation of the observation noise. By combining information from a forward and backward fixed-bandwidth notch filter, we were able to give a more accurate estimate of the observation noise during a step. The settling time of the KS is thus minimally affected by the poor performance of the fixed-band notch filter.

B. Influence PLI Amplitude

Results in Tables II, III, and Fig. 5(a) show that under stationary PLI conditions, the IAC and KS perform similarly well. In the absence of PLI the performance of the IAC is slightly better (S_{out} is 38 dB for the IAC and 37 dB for the KS), while for a constant PLI amplitude, the performance of the KS is slightly better (S_{out} is 34 dB for the IAC and 37 dB for the KS). Regardless of S_{in}, performance of both IAC and KS is substantially better compared to the performance of IIR and KF (S_{out} is 20 and 17 dB, respectively).

Since the attenuation of IIR is -70 dB at the PLI frequency, the performance of IIR does not depend on S_{in} and the lower performance of IIR is due to ringing caused by the QRS complexes. The lower performance of the KF is because the model parameters are adapted to the QRS complexes, leading to distortion of the ECG waveform. Since KF is a causal filter, in particular, the QRS complex and T-wave are distorted, as is seen from Tables II and III. Unlike KF, in IAC and KS, the learning rate is reduced during a QRS complex to prevent QRS complexes from interfering with the parameter estimation. As a result, under stationary PLI conditions, the QRS complex and T-wave are hardly distorted after filtering with IAC and KS.

For a PLI with sinusoidal modulated amplitude, the performance of all adaptive filters (IAC, KF, and KS) depends on S_{in}, as shown in Fig. 5(b). In this case, the PLI amplitude changes continuously, and thus, PLI parameters also need to be adapted continuously. As S_{in} decreases, the amplitude of the sinusoidal modulation increases and hence the PLI amplitude changes more rapidly. In particular, IAC and KF shows poor performance for low S_{in} (respectively, 7 and 9 dB at $S_{\text{in}} = -20$ dB).

As a consequence of the continuous variation in PLI amplitude, reducing the learning rate during a QRS complex results in an error in the estimation of the PLI amplitude. As S_{in} decreases, this error increases, leading to a decrease in S_{out}. Although both IAC and KS reduce parameter adaptation during a QRS complex, for the KS, the error in the estimation of the amplitude after each QRS complex is corrected for by the backward smoothing. This effect is reflected by the relatively high S_{out} of the P-wave and T-wave with respect to S_{out} of the QRS complex, as shown in Table IV. As a result, the KS performs well ($S_{\text{out}} = 30$ dB)

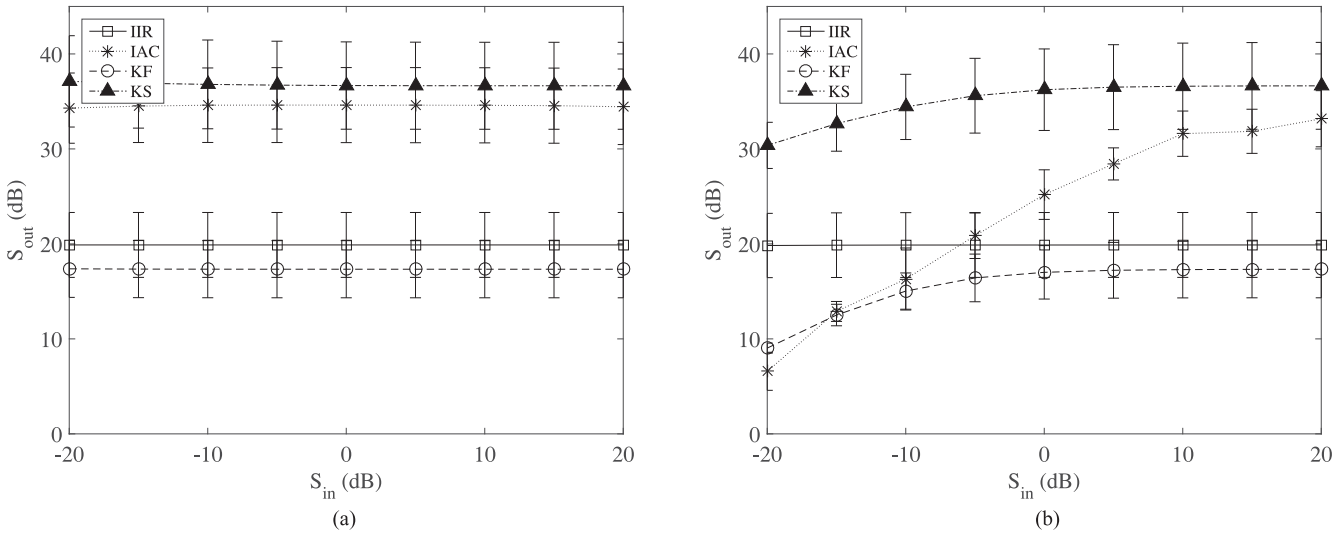

Fig. 5. Influence of PLI amplitude on S_{out}. PLI was simulated with $\Delta f = 0$ Hz. (a) Constant amplitude. (b) Sinusoidal modulated amplitude.

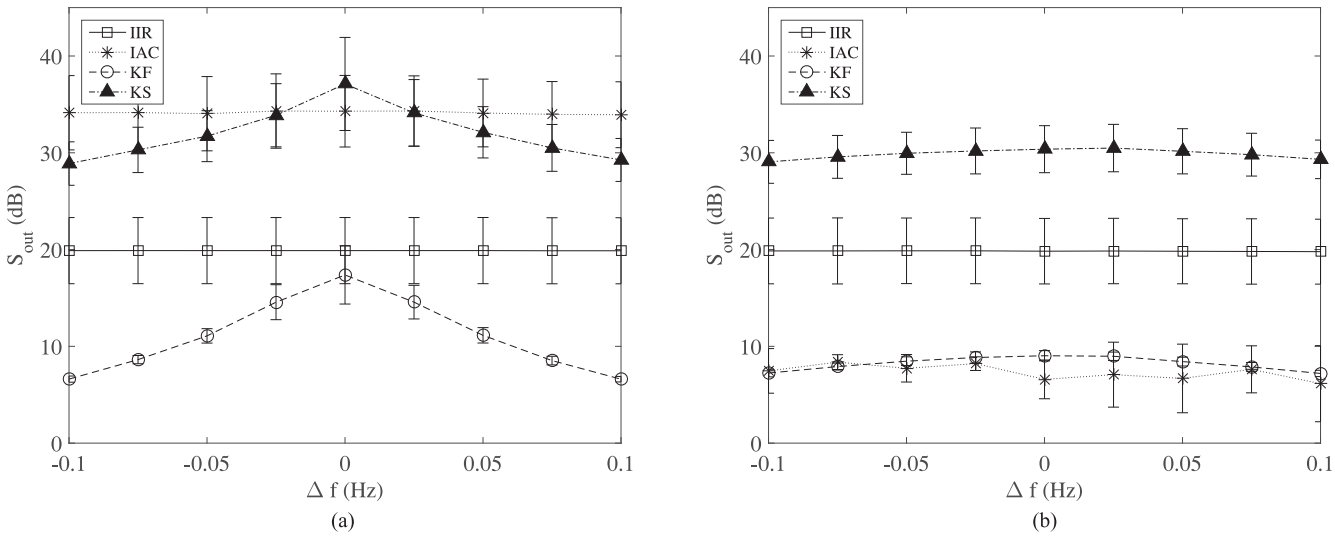

Fig. 6. Influence of frequency deviation from the PLI frequency on S_{out}. PLI was simulated for $S_{\mathrm{in}} = -20$ dB. (a) Constant amplitude. (b) Sinusoidal modulated amplitude.

even in case of $S_{\mathrm{in}} = -20$ dB and performance is significantly better compared other filters.

C. Influence PLI Frequency Deviation

In Fig. 6, the influence of deviating the frequency from the theoretical PLI frequency is shown on the S_{out}. Although according to the power system quality standards frequency deviations are typically limited to ± 0.01 Hz [13], we simulated frequency deviations up to ± 0.1 Hz.

From Fig. 6, it is observed that frequency deviations have little effect on the performance of IIR and IAC. Since for IIR the stopband was set to 48–52 Hz, no effect was expected. Besides, IAC was developed to track changes in frequency deviations and also no effect was expected for IAC.

In contrast to IIR and IAC, performance of the KF and KS is affected by varying the PLI frequency from the frequency that is assumed by the model of the KF and KS. Since for KS parameter adaptation is reduced during a QRS complex, the estimated PLI during a QRS complex is mostly determined by previous estimates and less by observations of the PLI. This means that, if the frequency of the model differs from the frequency of the observed PLI, the phase of the estimated PLI differs from the phase of the observed PLI after each QRS complex. As the frequency deviation increases, this phase difference increases and S_{out} decreases.

Instead of assuming a fixed PLI frequency, for future work, it might be interesting to develop a KS for a model that includes the PLI frequency as a separate model parameter. Note, however, that in this case the expression in (2) would no longer be valid and the model becomes nonlinear [10].

Despite the dependence of the performance of the KS on the frequency deviation, our simulations show that the KS outperforms other algorithms, even up to frequency deviations of

± 0.1 Hz. Although for a PLI with constant amplitude and frequency deviation of ± 0.1 Hz IAC has a better S_{out} (S_{out} is 35 dB for the IAC and 29 dB for the KS), the S_{out} for a PLI with sinusoidal modulated amplitude is much worse (S_{out} is 7 dB for the IAC and 29 dB for the KS).

D. Computational Complexity

The computational complexity of the KS depends on the time delay used for the filter (τ^{fb} and τ). Since for each new sample, the smoothing needs to be performed over the entire delay, increasing the delay substantially contributes to the complexity. For the selected time delays in this study, the computation complexity was in the order of 10^3 MPS. In contrast, IAC and KF are causal filters and their MPS is much smaller (39 and 50 MPS, respectively).

Despite the relatively high computational complexity with respect to the causal filters, at a sampling rate of 500 Hz, the KS still only requires about 10^6 multiplications per second. Assuming that the clock frequency of a modern DSP is in the order of gigahertz (e.g., C6000 series by Texas Instruments, Dallas, TX, USA), the KS only requires 0.1% of the entire capacity of the DSP. Therefore, real-time implementation of the KS should not be a problem.

For offline applications, it is possible to use a fixed-interval KS as an alternative to a fixed-lag KS [14]. Instead of calculating smoothed estimates for a fixed time lag τ, the fixed-interval KS gives smoothed estimates based on all observations in the signal. The fixed-interval KS first runs the forward KF over the entire signal, after which smoothed estimates are obtained by a backward KS. Since this approach only requires a single forward and backward run, the computational complexity reduces to 129 MPS.

VI. Conclusion

In this study, a linear fixed-lag KS was developed to suppress PLI in ECG recordings. The developed KS outperforms other methods that have been proposed in the literature in terms of step response settling time and output SNR. The proposed method can be used for semi real-time applications with a time delay of 0.4 s.

References

[1] W. Chen *et al.*, "A design of power supply for neonatal monitoring with wearable sensors," *J. Ambient Intell. Smart Environ.*, vol. 1, no. 2, pp. 185–196, 2009.

[2] S. Pei and C. Tseng, "Elimination of AC interference in electrocardiogram using IIR notch filter with transient suppression," *IEEE Trans. Biomed. Eng.*, vol. 42, no. 11, pp. 1128–1132, Nov. 1995.

[3] P. Hamilton, "A comparison of adaptive and nonadaptive filters for reduction of power line interference in the ECG," *IEEE Trans. Biomed. Eng.*, vol. 43, no. 1, pp. 105–109, Jan. 1996.

[4] B. Widrow *et al.* "Adaptive noise cancelling: principles and applications," *Proc. IEEE*, vol. 63, no. 12, pp. 1692–1716, Dec. 1975.

[5] J. Glover Jr, "Adaptive noise canceling applied to sinusoidal interferences," *IEEE Trans. Acoust., Speech, Signal Process.*, vol. 25, no. 6, pp. 484–491, Dec. 1977.

[6] Y. Ider and H. Köymen, "A new technique for line interference monitoring and reduction in biopotential amplifiers," *IEEE Trans. Biomed. Eng.*, vol. 37, no. 6, pp. 624–631, Jun. 1990.

[7] A. Ziarani and A. Konrad, "A nonlinear adaptive method of elimination of power line interference in ECG signals," *IEEE Trans. Biomed. Eng.*, vol. 49, no. 6, pp. 540–547, Jun. 2002.

[8] S. M. Martens *et al.*, "An improved adaptive power line interference canceller for electrocardiography," *IEEE Trans. Biomed. Eng.*, vol. 53, no. 11, pp. 2220–2231, Nov. 2006.

[9] R. Sameni, "A linear Kalman notch filter for power-line interference cancellation," in *Proc. CSIInt. Symp. Artificial Intell. Signal Process.*, 2012, pp. 604–610.

[10] P. K. Dash *et al.*, "An extended complex Kalman filter for frequency measurement of distorted signals," *IEEE Trans. Instrum. Meas.*, vol. 49, no. 4, pp. 746–753, Aug. 2000.

[11] S. Butterworth, "On the theory of filter amplifiers," *Wireless Engineer*, vol. 7, no. 6, pp. 536–541, 1930.

[12] J. Stinstra *et al.*, "Multicentre study of fetal cardiac time intervals using magnetocardiography," *Brit. J. Obstetrics Gynaecol.*, vol. 109, pp. 1235–1243, Nov. 2002.

[13] D. Fink and H. Beaty, *Standard Handbook For Electrical Engineers*. New York, NY, USA: McGraw-Hill, 1987.

[14] A. Gelb, *Applied Optimal Estimation*. Cambridge, MA, USA: MIT Press, 1974.

[15] M. Niedźwiecki, "Generalized adaptive notch smoothing revisited," *IEEE Trans. Signal Process.*, vol. 58, no. 3, pp. 1565–1576, Mar. 2010.

[16] B. Anderson and J. Moore, *Optimal Filtering*, Englewood Cliffs, NJ, USA: Prentice-Hall, 1979.

[17] J. de Freitas *et al.*, "Hierarchical Bayesian-Kalman models for regularisation and ARD in sequential learning," Cambridge University, Tech. Rep., CUED/F-INFENG/TR 307, 1998.

[18] R. Kalman, "A new approach to linear filtering and prediction problems," *J. Basic Eng.*, vol. 82, no. 1, pp. 35–45, 1960.

[19] B. Kohler *et al.*, "The principles of software QRS detection," *IEEE Eng. Med. Biol. Mag.*, vol. 21, no. 1, pp. 42–57, Jan./Feb. 2002.

[20] F. Gustafsson, "Determining the initial states in forward-backward filtering," *IEEE Trans. Signal Process.*, vol. 44, no. 4, pp. 988–992, Apr. 1996.

[21] R. Vullings *et al.*, "Dynamic segmentation and linear prediction for maternal ECG removal in antenatal abdominal recordings," *Physiol. Meas.*, vol. 30, no. 3, pp. 291–307, Mar. 2009.

[22] T. T. Tay *et al.*, *High Performance Control*, Boston, MA, USA: Birkhuser, 1997.

Authors' photographs and biographies not available at the time of publication